Discovery of Diffuse Hard X-ray Emission and Its Relation to High Energy Particles in the Massive Star Forming Region

Yuichiro Ezoe
ISAS/JAXA, 3-1-1 Yoshinodai, Sagamihara, Kanagawa, Japan
Yasunobu Uchiyama
Yale University, 260 Whitney Ave, New Haven, CT 06520, USA
Kazuo Makishima
University of Tokyo, 7-3-1 Hongo, Bunkyo-ku, Tokyo, Japan

Chandra data of the representative massive star-forming region NGC 6334 is analyzed. After removing newly detected 792 point sources, extended X-ray emission (5×9 pc^2 and 2×10^{33} ergs s^{-1} in the 0.5–8 keV luminosity) is found. By estimating unresolved point sources, $\sim$90% of the emission was concluded as diffuse in nature. In tenuous cloud regions, its spectra tend to be represented by thermal emission of several keV. In contrast, in more dense regions, they exhibit flat continua (a photon index of $\sim$1), suggesting bremsstrahlung emission by sub-MeV electrons. All the results can be explained in terms of strong shocks of stellar winds from young OB stars.

1. Introduction

Massive stars ($> 10\ M_\odot$) affect their environments profoundly by ultra-violet photons (10^{37-39} ergs s^{-1}) and fast stellar winds (1000-4000 km s^{-1} , 10^{34-37} ergs s^{-1}). Through exhaustive studies on massive star-forming regions (MSFRs) made with *Einstein* , *ROSAT* , and *ASCA* , one important issue has been suggested;“ a diffuse X-ray emission ”. However, because of limited angular resolution and sensitivity, it was difficult to conclude whether the apparently diffuse X-ray emission in MSFRs are really diffuse in nature. From theoretical viewpoint, such a phenomenon had long been expected in terms of shocks produced by fast stellar winds from the massive stars (e.g., [1]). If diffuse emission is true, what is the emission mechanism ? If the shock is responsible, do we expect not only thermal one but also non-thermal emission like that in supernovae ? Thanks to its superb angular resolution, *Chandra* first enabled a detailed examination of diffuse X-ray emission in MSFRs [2–4]. Here we report on the discovery of diffuse hard X-ray emission from the representative MSFR NGC 6334.

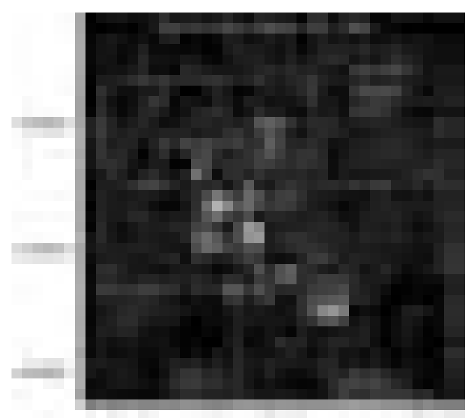

Figure 1: Near infrared image of NGC 6334 taken from the 2MASS (2μm All Sky Survey) atlas. Overlaid contours are CO J=2-1 [11]. Crosses and diamonds indicate positions of radio sources and FIR cores, respectively. Squares represent the two field-of-view of the *Chandra* observation. Co-ordinates are E1950.

2. Observation of NGC 6334

NGC 6334 is a nearby (1.7 kpc yielding a plate scale of $1''$ =0.01 pc; [5]) MSFR, with the bolometric luminosity 4×10^{39} ergs s^{-1} [6] and 6×10^{33} ergs s^{-1} in X-rays [7], which are one of the highest of this class. As shown in figure 1, it contains several star-forming sites defined in wide wavelength ranges; the far-infrared (FIR) cores I(N), I, II, III, IV, and V, the radio source A-F and a star cluster around the star N29. Not all of these are detected in both wavelength ranges (see figure 1). Each site is known to be powered by massive stars, either zero-age main-sequence stars or proto stars (e.g., [8–10]).

We conducted two 40 ksec ACIS–I observations of NGC 6334 with *Chandra* in 2002, to cover the whole nebula. Hereafter we call each of them “north field” and “south field”, according to their declinations. We started data reduction with the Level 1 event files provided by the *Chandra* X-ray Center, and followed the standard data reduction procedures using the Chandra Interactive Analysis of Observations software package version 2.3 and the calibration data base version 2.18. We corrected pulse heights for the Charge Transfer Inefficiency. After these data reductions, we have obtained 39.4 and 19.4 ksec exposure times in the north and south observations. Using these data, we created X-ray images as shown in figure 2. In this figure, we observe a number of point sources and also indication of extended structures.

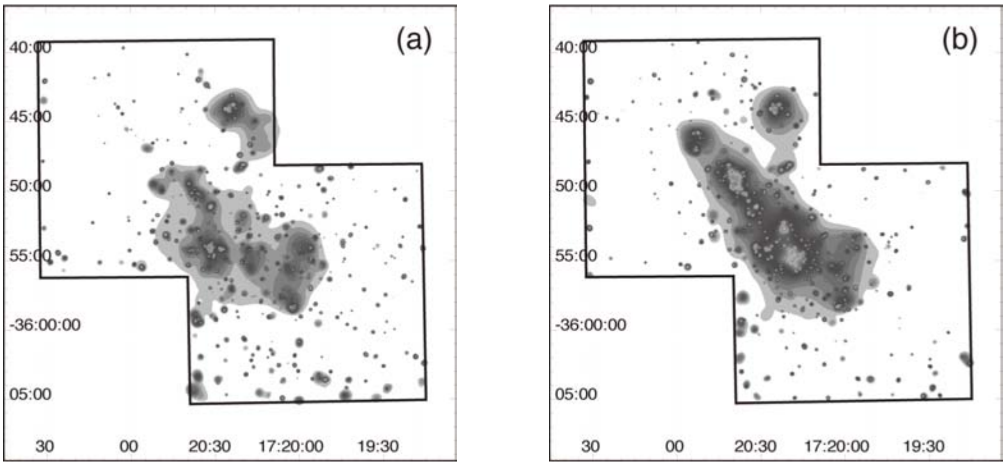

Figure 2: Adaptively smoothed X-ray images of NGC 6334 in the (a) 0.5–2 and (b) 2–8 keV bands, displayed on the J2000 coordinates.

3. Extended Emission Analysis

In order to examine the extended structure, we must first detect and exclude point sources. We then utilized the **wavdetect** program. We used images in three bands (0.5–2, 2–8, and 0.5–8 keV) independently. Significance criterion and wavelet scales were set as 1×10^{-6} and 1 to 16 pixels in multiples of 2, respectively. As a result, we have detected 449 and 390 sources in the north and south fields, respectively. Excluding overlaps, the total source number is 792. We estimated the completeness limit (CL) from source-number histograms as a function of background-subtracted counts. CL is $\sim$10-30 net-counts and increases toward the outside edge of the field of view. This CL corresponds to the 0.5–8 keV absorption-uncorrected luminosity of 2-6 and 4-12×10^{30} ergs s^{-1} in the north and south observations, respectively.

We then created point-source masks to remove point sources. We defined new circular regions around individual sources based on the "Chandra Ray Tracer". For each source, we chose a radius to include $\sim$ 98 % of photons at the Al Kα-line energy (1.497 keV). We applied obtained masks to raw CCD images, and then created the residual emission images as exhibited in figure 3.

In order to analyze the spectrum of the extended emission, we define in figure 3 a rectangle of $\sim 10' \times 18'$, elongated along the linearly aligned cores, and call it "extended emission region", or EER. Using the equilateral line from the two aimpoints, we further subdivide this EER into two trapezoids. When analyzing the north-eastern and south-western trapezoids, we use only the north and south field observation data, respectively. We obtained two sets of spectrum, arf, and rmf files corresponding to the two observations, and then added them together considering the difference in their exposure times. Also, we have chosen two square background regions (BR) where the extended emission is relatively weak in the north and south fields. We then similarly derived a background spectrum. The 0.5–7 keV raw counts of the EER and BR spectra are 22500±150 and 14600±160, respectively, yielding the excess counts of 7900±220. Thus, the excess emission is statistically quite significant.

To characterize the spectrum of the background-subtracted EER emission, we conducted spectral fitting to the EER spectrum. We employed a simple power-law model with an interstellar absorption. The results are shown in table I and figure 4. All quoted errors in the spectral fitting refer to 90 % confidence levels. The fit was not acceptable with $\chi^2/\nu \sim 2$ because of an excess around 2–3 keV, although it contributes only $\sim$5% in the 0.5–7 keV flux. The spectrum shows no emission lines and show very flat continuum with $\Gamma \sim 0.9$. The 0.5–8 keV flux implied by the best-fit model is 5.6×10^{-12} ergs s^{-1} cm^{-2}before removing the absorption, and the absorption-corrected 0.5–8 keV luminosity reaches 2×10^{33} ergs s^{-1} .

To examine a contribution of unresolved faint sources, we utilized the absorption-uncorrected luminosity function of 548 point sources in the EER. To complement the luminosity function below the CL, we have incorporated *Chandra* results on the Orion Nebula Cluster (ONC) taken from Feigelson et al. (2002) [12]. We corrected the ONC function for the absorption and source number density. We estimated the expected flux of unresolved sources by integrating the luminosity function of the ONC, from the completeness limit down to the end, $\sim 10^{28}$ ergs s^{-1} . The estimated unresolved sources are 2500 in number and $\sim2\times10^{32}$ ergs s^{-1} in absorption-uncorrected luminosity. This is only 12 % of the EER emission. Hence, we conclude a large part of the emission is truly diffuse.

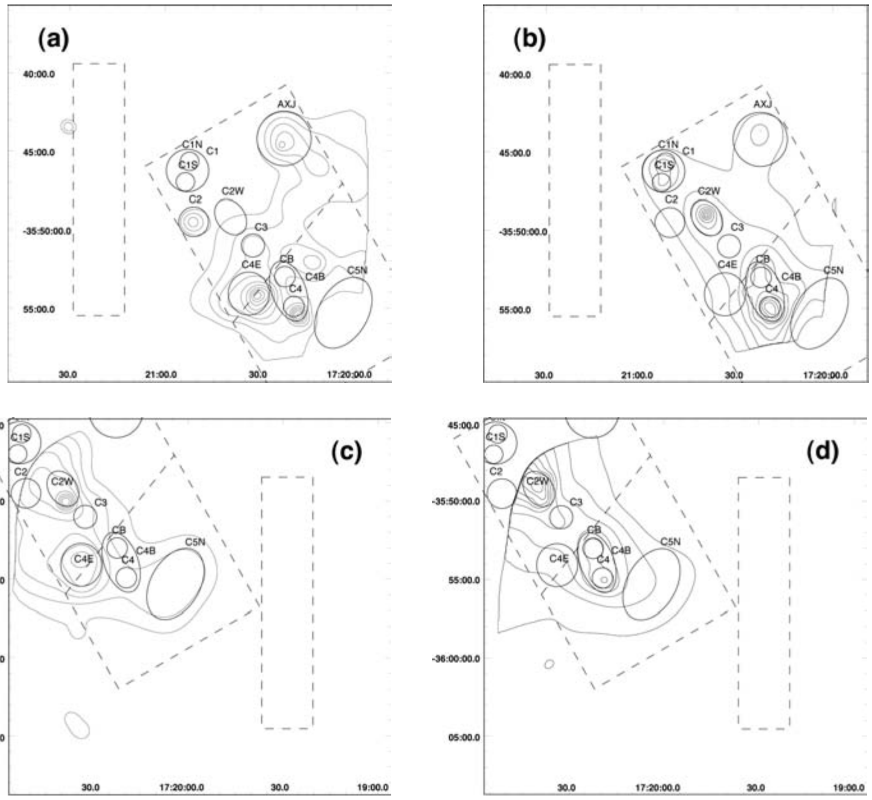

Figure 3: Adaptively smoothed images of the extended emission, plotted with contours in logarithmic scales. Panels (a) and (c) show the soft band images, while (b) and (d) the hard band. Also two pairs of panels (a) and (b), and, (c) and (d), correspond to the north and south field, respectively. Two trapezoids and squares represent the EER and BR, respectively. Circles and ellipses indicate the selected regions to be utilized in the spectral analysis.

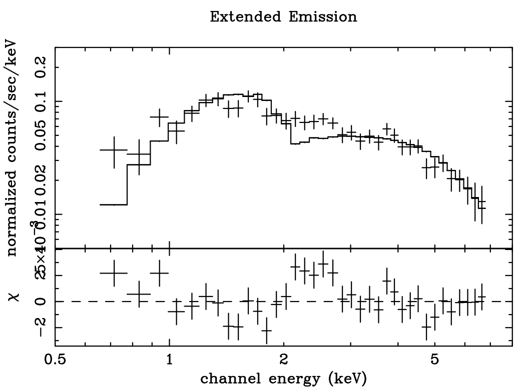

Figure 4: The ACIS–I spectrum of the EER, compared with the best-fit power-law model (solid line). See table I for the obtained parameters.

Table I Parameters derived by the power-law model fitting to the EER spectrum.

model	param	
abs.[a]	$N_{\rm H}$	$0.42^{+0.17}_{-0.18}$
P.L.[b]	Γ	$0.85^{+0.17}_{-0.19}$
	norm	$4.4^{+1.1}_{-1.0} \times 10^{-4}$
	$F_{\rm X}$	$5.6{\times}10^{-12}$
	$L_{\rm X}$	$2.2{\times}10^{33}$
χ^2/ν		64.4 / 34

[a] The hydrogen column density in 10^{22} cm^{-2}.
[b] Power-law model. Γ is the photon index, norm is photon flux at 1 keV in photons cm^{-2} s^{-1}, $F_{\rm X}$ and $L_{\rm X}$ are the X-ray flux and absorption-corrected luminosity in the 0.5–8 keV band, respectively.

4. Region-by-region Spectral Analysis

4.1. Region definition

We then consider the apparently flat spectrum of the EER ($\Gamma \sim 0.9$). If it arises from non-thermal emission, the discovery would be of great importance, since the X-ray emission from MSFRs are considered as a thermal one. Nevertheless, superposition of thermal components with different absorptions which also makes apparently a flat spectrum, must be examined. Hence, we conducted region-by-region spectral analysis. Based on the extended emission images as shown in figure 3, we newly select 12 bright clumps; C1, C1N, C1S, C2, C2W, C3 and AXJ in the north field, and, C4E, C5N, C4B, CB and C4B in the south field. C stands for "core" and corresponds to the FIR cores, while AXJ the known X-ray source AXJ 1720.4−3544.

4.2. Spectral fitting of the summed point sources

We first analyzed the summed point sources with simple models. The spectra in 8 out of the 12 regions have been represented successfully by a single temperature thin-thermal model. The C2W and C3 region required an additional narrow Gaussian and a second thermal plasma model of rather low temperature, respectively. The CB and C4B which involve the bright background AGN (NGC 6334 B), a power-law model and a single temperature plus power-law model, respectively, gave acceptable fits. All the 12 spectra have been successfully reproduced in this way. Fitting results are summarized in figure 5 (a).

The obtained absorption column density differs clearly from region to region. Specifically, the AXJ, C2, C3, C4, C5N regions have column densities of $(0.5 \sim 1) \times 10^{22}$ cm^{-2}, while the others have $(2 \sim 10) \times 10^{22}$ cm^{-2}. The derived temperatures are moderately high, i.e., several keV, in agreement with the typical X-ray temperature of young stellar objects. All the spectra except those from the three regions C3, CB and C4B have been successfully reproduced each by a single temperature plasma model absorbed by a single column density. This fitting result ensures that each of the 12 regions has a well-defined value of $N_{\rm H}$.

4.3. Spectral fitting of the diffuse emission

Next we conducted spectral fitting of the diffuse emission in each region. We fitted spectra with a single temperature plasma model. The temperature and the column density were left free to vary except in C1, C1N, C1S, C2W, C4, and CB regions for which the column density is fixed at that of the summed point sources due to the paucity of the signal. The heavy element abundances were fixed at 0.3 solar except in C1 and C1S for which it was left free to reproduce a sign of Fe-K line emission. Escape photons from the summed point sources were taken into account by adding their best-fit models, and multiplying it with the third-order polynomial function.

The results of this analysis are shown in figure 5 (b). All the fits have been acceptable, although the C4B fit is marginally acceptable ($\chi^2/\nu = 61.9/44$) because of the data excess in 1–2 keV as shown in figure 6 (left). We then found that, in weakly absorbed regions, the best-fit temperatures are moderate (<10 keV). On the other hand, in strongly absorbed ones (hard regions), the temperatures tend to higher. Especially, in C4, CB, and C4B regions, the best-fit values far exceed 10 keV. Considering that these spectra show no emission lines, we then refitted them by a power-law model. For example, in the case of the most photon-rich spectrum of C4B (730 cts), we obtained a better fits ($\chi^2/\nu = 54.3/44$) as seen in figure 6 (right). The obtained power-law indices are extremely small ($0.39^{+0.66}_{-0.63}$) with $\mathrm{N_H} = 1.7^{+1.2}_{-1.0}$ cm^{-2}. We also tested a leaky-absorber model (a single emission with two different absorptions) for the C4B spectrum but the temperature is still high (>10 keV). Similar to C4B, the other two (C4 and CB) show flat continua with $\Gamma \sim 0.6 - 1.0$ with 90 % confidence upper limits of $\sim$ 1.5 Hence, the apparently flat spectrum of the diffuse emission is a mixture of thermal and very flat continuum spectra. Although the thermal plasma picture cannot be totally rejected, the latter favors non-thermal emission.

5. Discussion

We have revealed the existence of the diffuse hard X-ray emission in NGC 6334. In tenuous part of the molecular clouds, the diffuse spectra show thermal plasma emission with temperatures of several keV. In dense molecular cloud cores, we have found flat-continuum spectra with $\Gamma \lesssim 1.5$. The observed diffuse X-rays can be a mixture of thermal and non-thermal emission. Below we examine the two possibilities considering emission mechanism, and constrain on necessary energy to be supplied.

In the non-thermal emission case, there can be three emission mechanism candidates; bremsstrahlung, inverse Compton, and synchrotron emission. Based on the standard diffusive acceleration theory, the latter two can be ruled out since the electron and photon spectra cannot be flatter than 2 and 1.5, respectively [13]. On the other hand, in an environment with a high matter density like in the present case, the spectrum of energetic electrons will become flatter than is implied by the theory, because lower-energy electrons lose energy more quickly than the more energetic ones [14]. However, because the Coulomb loss overwhelms the bremss in this energy range, a luminosity of at least 10^{36} ergs s^{-1} is required to each hard X-ray clump of NGC 6334.

In case of thermal plasmas, the emission mechanism is considered as thermal bremsstrahlung with fluorescent lines. We can calculated plasma parameters including the total energy to be supplied from observational quantities. Here we assume parameters of a typical soft region ($L = 5 \times 10^{31}$ ergs s^{-1} , $kT = 5$ keV, and a radius of 0.5 pc) and the age of NGC 6334 (~1 Myr). We also assume the filling factor η. Then, the energy input can be calculated as $10^{33}\eta^{\frac{1}{2}}$ ergs s^{-1}

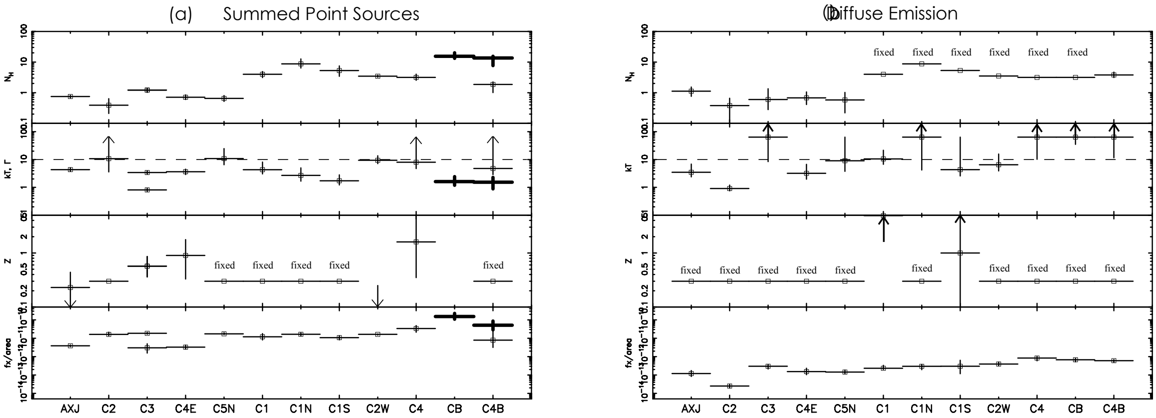

Figure 5: Results of the spectral fitting to (a) the summed point sources and (b) the diffuse emission in the 12 diffuse emission regions with a single temperature model (boxes), or a power-law model (thick crosses), or a combination of them. From top to bottom panels, plotted are the best-fit values of the absorption column density in 10^{22} cm^{-2}, the temperature in keV, the abundance in solar units, and the uncorrected 0.5–8 keV X-ray surface brightness in ergs s^{-1} cm^{-2}pc^{-2}. Dashed line indicates the temperature of 10 keV.

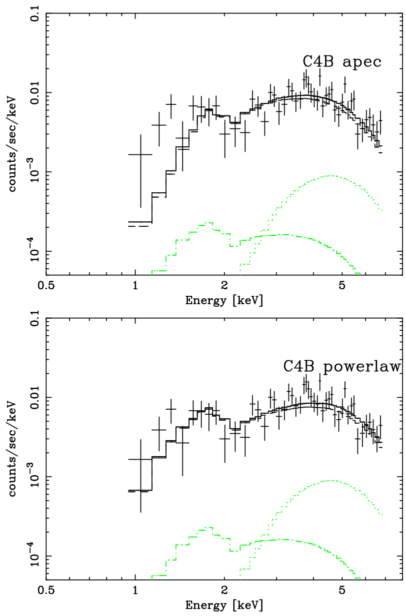

Figure 6: The C4B spectrum fitted with a single temperature plasma model and a power-law model (solid lines). The escape-photon effect (2% at Al K_α) from the summed point sources are included (dashed lines).

for each soft region. If scaling to the whole EER emission, this increases to be $10^{36}\eta^{\frac{1}{2}}$ ergs s^{-1} . The cooling time will be $\sim 10^8\eta^{\frac{1}{2}}$ yr, far larger than the typical age of MSFRs (10^{5-6} yr). Thus, the total energy will be all what is to be supplied during this time scale.

We here must examine whether the plasma can be confined or not, since pressure of the thermal plasma as estimated above based on the thermal assumption is higher than that of the surrounding molecular clouds (10^{5-6} K cm^{-3}) and the U can be underestimated in such situation. In fact, a 5 keV plasma can expand (with sound velocity) over $\sim$ 0.5 pc in only $\sim$ 1000 yr, which is much shorter than the cooling time scale. However, the confinement of the plasma is possible by the surrounding dense HII region, where the pressure is thought to be higher ($10^7 \sim 10^8$ K cm^{-3}, [8]). This roughly agrees with the observed distribution of the diffuse emission. There is also an other possibility, the magnetic pressure of the molecular cloud, which is also large enough to confine the plasma if assuming the magnetic field strength of the cloud cores (an order of 100μ G, [15]).

What explains the huge energy necessary in both cases ? Among many energetic phenomenon associated with MSFRs, the most plausible candidate is the fast stellar wind from massive OB stars. We know that NGC 6334 involves at least 8 late O or early B-type stars. Such a star is expected to emit thick and fast winds, individually supplying a kinematic luminosity of 10^{35} erg/s. By assuming a few such stars, we can explain the energy input in both two interpretations. The maximum temperature behind the shock can explain the observed temperature 1$\sim$10 keV since the fast stellar wind reaches 1000-4000 km s^{-1} . Furthermore, the high energy particle accelerated at the shock front is possible. The size of the whole diffuse emission of NGC 6334 (5$\times$9 pc^2) can be explained by a superposition (8 or more) of OB stars [1].

Finally, we summarize the reported X-ray luminosity of the diffuse X-ray emission $L_{\rm diffuse}$ in MSFRs with *Chandra* as a function of a bolometric luminosity $L_{\rm bol}$. Although the lack of data points in the low $L_{\rm diffuse}$ and the large $L_{\rm bol}$ range could be a selection effect, we see a sign of positive correlation. Since the most of $L_{\rm bol}$ is due to OB stars in individual MSFRs, this relationship independently suggests a close relationship of the emission to the massive stellar ac-

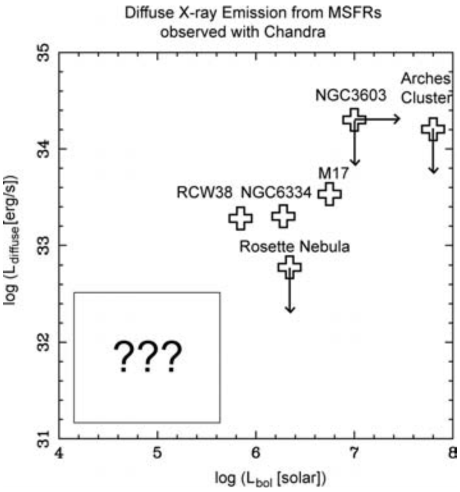

Figure 7: The bolometric luminosity versus the 0.5–8 keV X-ray luminosity of diffuse X-ray emission in MSFRs observed with *Chandra* (see [3-4] for the summary of the reported diffuse X-ray luminosity).

tivities such as their fast stellar winds. In order to strengthen this indication, we should further analyze the *Chandra* of low $L_{\rm bol}$ MSFRs.

In summary, our Chandra results on NGC 6334 provide a strong support to a view that the strong stellar winds from young OB stars give rise to the diffuse hard X-ray emission.

References

[1] J.E. Dyson and J. de Vries 1972, A&A, 20, 223
[2] S.J. Wolk et al. 2002, ApJL, 580, L161
[3] L. K. Townsley et al. 2003, ApJ, 593, 874
[4] L. K. Townsley et al. 2004, astroph/0406349
[5] T. Neckel 1978, A&A, 69, 51
[6] L. Loughran 1986, ApJ, 303, 629
[7] Y. Sekimoto 2000, PASJ, 52, L31
[8] L. F. Rodriguez 1982, ApJ, 255, 103
[9] P. M. Harvey and I. Gatley 1983, ApJ, 269, 613
[10] S. M. Straw et al. 1989, ApJS, 69, 99
[11] K. E. Kraemer et al. 1999, ApJ, 516, 817
[12] E. D. Feigelson et al. 2002, ApJ, 574, 258
[13] M. S. Longair 1994, "High Energy Astrophysics", Cambridge University Press, UK
[14] Y. Uchiyama 2002, ApJ, 571, 866
[15] A. P. Sarma et al. 2000, ApJ, 533, 271